AGU ADVANCING EARTH AND SPACE SCIENCE

Earth and Space Science

RESEARCH ARTICLE
10.1029/2022EA002319

Maritime Aerosol and CCN Profiles Derived From Ship-Based Measurements Over Eastern North Pacific During MAGIC

Jordann Brendecke[1], Xiquan Dong[1], Baike Xi[1], and Xiaojian Zheng[1]

[1]Department of Hydrology and Atmospheric Sciences, University of Arizona, Tucson, AZ, USA

Key Points:

- Aerosols have little longitudinal variation during MAGIC except over the coastal region near California
- CCN retrieval methods developed in Ghan and Collins (2004) and Ghan et al. (2006) are used in this study for the MAGIC campaign
- CCN has the highest correlation with cloud-droplet number concentration near cloud base in non-drizzling clouds under coupled conditions

Supporting Information:

Supporting Information may be found in the online version of this article.

Correspondence to:

X. Dong,
xdong@arizona.edu

Citation:

Brendecke, J., Dong, X., Xi, B., & Zheng, X. (2022). Maritime aerosol and CCN profiles derived from ship-based measurements over Eastern North Pacific during MAGIC. *Earth and Space Science*, *9*, e2022EA002319. https://doi.org/10.1029/2022EA002319

Received 11 MAR 2022
Accepted 28 MAR 2022

Author Contributions:

Conceptualization: Xiquan Dong
Formal analysis: Xiquan Dong, Baike Xi
Funding acquisition: Xiquan Dong
Investigation: Jordann Brendecke
Methodology: Jordann Brendecke
Project Administration: Xiquan Dong
Software: Jordann Brendecke, Xiaojian Zheng
Supervision: Xiquan Dong, Baike Xi
Validation: Xiquan Dong, Baike Xi
Visualization: Jordann Brendecke
Writing – original draft: Jordann Brendecke

Abstract Atmospheric aerosols are widely recognized to give rise to a substantial radiative forcing to the climate by scattering and absorbing radiation and by modifying the microphysical, lifetime, and radiative properties of clouds. During the Marine ARM GPCI Investigation of Clouds (MAGIC) over the Eastern North Pacific (ENP), the ship-based measured cloud condensation nuclei (CCN) concentration at 0.2% supersaturation ($N_{CCN,0.2}$) and condensation nuclei concentration (N_{CN}) had mean values of 116.7 and 219.4 cm^{-3}, with the highest concentrations found closest to LA due to an increase in aerosol sources. Moving westward, both $N_{CCN,0.2}$ and N_{CN} gradually decreased until stabilizing near 100 cm^{-3} and 200 cm^{-3}, respectively. Using the methods proposed by Ghan and Collins (2004), https://doi.org/10.1175/1520-0426(2004)021<0387:uoisdt>2.0.co;2 and Ghan et al. (2006), https://doi.org/10.1029/2004jd005752, $N_{CCN,0.2}$ profiles are retrieved using the surface measured $N_{CCN,0.2}$ as a constraint. For coupled conditions, correlations between the retrieved $N_{CCN,0.2}$ profiles and cloud-droplet number concentration (N_C) increase from 0.26 at the surface to 0.38 near cloud base, particularly true for non-drizzling clouds. Although the correlations are lower than expected, the percentage increase (46.2%) is encouraging. Finally, the relationships between cloud breakup (CB) and the stratocumulus to cumulus transition (SCT) with environmental conditions and associated aerosols are also studied. The decreased N_{CN} trend east of CB is mainly caused by precipitation scavenging, while the increased N_{CN} trend west of CB is strongly associated with the increased surface wind speed and fewer drizzle events. A further study is needed using high-resolution models to simulate these events.

1. Introduction

Atmospheric aerosols are widely recognized to give rise to a substantial radiative forcing of climate by scattering and absorbing radiation (direct effects) and by modifying the microphysical, optical, and radiative properties of clouds, affecting their reflectivity and persistence (indirect effects). One example of the aerosol indirect effects (AIEs) is Marine Cloud Brightening (MCB, Latham et al., 2012). The basic principle behind the idea is to seed marine stratocumulus clouds with numerous aerosols generated at or near the ocean surface. These particles would have a sufficiently large salt mass to ensure their activation and subsequent growth within the clouds, but not large enough to generate drizzle or precipitation. Moreover, these particles would be sufficiently numerous to enhance the cloud-droplet number concentration (N_C) to values substantially higher than the natural ones. This will result in two effects: (a) the marine boundary layer (MBL) cloud droplets become smaller and thus the MBL clouds are more reflective of incoming solar radiation (Twomey, 1977), and (b) the MBL clouds become more persistent, occupy a broader areal extent, and suppress precipitation (Albrecht, 1989). Both effects reduce the amount of solar radiation reaching the Earth's surface and therefore have a cooling effect on the planet.

Understanding how aerosols influence MBL clouds remains vital in determining cloud properties and lifecycle. Each cloud droplet requires an aerosol particle to initiate growth by condensation in the real atmosphere; however, factors including the aerosol size, chemistry, and meteorological condition will determine whether a particle will become activated to allow condensation (Kohler, 1936; Zheng et al., 2020). Aerosol particles which satisfy these conditions at a given supersaturation are known as cloud condensation nuclei (CCN). Theoretically, CCN number concentrations (N_{CCN}) increase monotonically with increasing supersaturation until all condensation nuclei (CN) are activated. Hence, measurements of N_{CCN} as a function of supersaturation can provide important information on the relationship between aerosols and clouds. It has long been hypothesized that aerosol concentration can affect cloud-droplet number concentration (N_C) and cloud albedo (Twomey, 1977). N_{CCN} will also influence cloud-droplet effective radius (r_c), further affecting cloud to drizzle initiation when cloud droplets outweigh the updraft buoyancy force for drizzle to begin. Moreover, Yamaguchi et al. (2017) found that drizzle rates can affect the cloud's lifetime and the transition from stratocumulus to cumulus clouds. These indirect aerosol effects

Writing – review & editing: Jordann Brendecke, Xiquan Dong, Baike Xi, Xiaojian Zheng

remain a critical key in simulating MBL clouds (Wang et al., 2020). To fully understand aerosol indirect effects, it's important to understand how aerosol properties, especially near cloud base, change with time under different atmospheric conditions, such as strong and weak wind speeds, coupled and decoupled boundary layers.

Multiple field campaigns around the world have been conducted to better understand aerosol properties and their interactions with clouds over different oceanic regions. This paper will focus on the aerosol and cloud properties collected during the Marine ARM GPCI Investigation of Clouds (MAGIC) over the Eastern North Pacific (ENP). The purpose of this study is to investigate the longitudinal variations and vertical distributions of aerosol properties, and their relations with cloud properties presented in Brendecke et al. (2021). In this campaign, the Horizon Lines cargo ship, *Spirit*, was used to board atmospheric instrumentation to measure aerosol and cloud properties as the ship traveled to and from Los Angeles, California and Honolulu, Hawaii. Over this region, MBL clouds typically transitioned from stratocumulus (closed-cell) to cumulus (open-cell) moving westward. Although there were multiple remote sensors for observing MBL cloud and precipitation properties during the MAGIC field campaign, there were no aircraft in situ measurements to provide the vertical profiles of MBL cloud and drizzle microphysical properties. Brendecke et al. (2021) implemented the methods of Wu et al. (2020) to retrieve MBL cloud and drizzle microphysical properties during MAGIC using ship-based observations. Wu et al. (2020) developed innovative methods to decompose drizzle and cloud reflectivity in a cloud layer from ARM cloud radar measurements and then simultaneously retrieve cloud and drizzle microphysical properties during Aerosol and Cloud Experiments in the Eastern North Atlantic (ACE-ENA) field campaigns (June–July 2017 and January–February 2018). These ground-based retrievals were then validated by aircraft in situ measurements during ACE-ENA in which the uncertainties of MBL cloud and drizzle retrievals were estimated.

In addition to the MBL cloud and drizzle property retrievals, different methods to retrieve the vertical profiles of aerosol concentration have been developed from other campaigns based on ground-based observations. Knowing how these aerosols change with height is critical because aerosols below cloud base will ultimately influence the cloud properties aloft. Understanding the aerosol properties near cloud base will improve our knowledge on the representation of aerosol indirect effects because most of the previous studies (e.g., Dong et al., 2015; Zheng et al., 2020, 2022) used surface aerosols or CCN information to study the aerosol and cloud interactions (ACIs). These studies assumed that the surface CCN concentrations are the same as those near cloud base. This assumption may be valid for coupled meteorological conditions but may not be for decoupled conditions (Dong et al., 2015). This study uses the method developed by Ghan and Collins (2004) and Ghan et al. (2006) to retrieve N_{CCN} profiles from the surface to cloud base during MAGIC using lidar backscatter, aerosol humidification factor, relative humidity profiles, and surface measured N_{CCN}. While other methods were proposed by Feingold and Grund (1994) and Lv et al. (2018) to obtain N_{CCN} profiles, those methods are either based on Junge power-law aerosol size distribution (Junge, 1952) or instrumentation not available during the MAGIC campaign. In this study, in situ measured N_{CCN} onboard the ship is used to constrain the retrieved N_{CCN} profiles to keep consistent between surface measurements and retrieved profiles.

The primary goal of this study is to investigate the longitudinal variations and vertical distributions of aerosol properties and their relations with cloud properties over ENP during MAGIC. Through an integrative analysis of the ship-based N_{CCN} measurements and the retrieved N_{CCN} profiles, we can have a better understanding of previous assumptions in ACI studies. That is, whether or not the surface N_{CCN} is the same as the N_{CCN} at or near cloud base? Under what environmental conditions, they agree or not agree? The MBL cloud properties in Brendecke et al. (2021) are used to study the relations between aerosols and clouds. The outline of this manuscript is as follows: a brief introduction of the instrumentation used during MAGIC, and the retrieval method of N_{CCN} profile will be given in Section 2. Section 3 will provide an analysis and discussion of the results. This section will consist of four subsections: the overall in-situ measurements, analysis of the retrieved results, estimation of uncertainties, and the causes and effects between aerosols and the stratocumulus to cumulus transition (SCT). Finally, a summary of the results and potential future work will be given in Section 4.

2. Data and Methodology

The MAGIC field campaign was conducted from October 2012 to September 2013 to better understand subtropical MBL aerosols, clouds and ACIs, and the environmental factors controlling the SCT. Both in situ and remotely sensed instrumentation from Atmospheric Radiation Measurement (ARM) mobile facility (Mather &

Voyles, 2013; Miller et al., 2016) were placed onboard the ship traversing back and forth from Los Angles, California (LA, 33.7°N, −118.2°E) and Honolulu, Hawaii (HI, 21.3°N, −157.8°E). Unlike most other ARM field campaigns, MAGIC was operated over a large area coverage, ∼4,000 km from LA to HI, and across multiple seasons. A total of 20 round trips were conducted with westward-moving portions labeled "LegxxA" as clouds transitioned from stratocumulus to cumulus and eastward-moving portions labeled "LegxxB," denoting the opposite transition of clouds.

The primary measurements used in this study are from the CCN particle counter (CCNPC), condensation particle counter (CPC), radiosonde soundings, and high spectral resolution lidar (HSRL). A full list of instrumentation during MAGIC can be found at https://www.arm.gov/research/campaigns/amf2012magic. A brief description of the retrieval instrumentation and a summary of the retrieval methods will be followed.

2.1. Instrumentation

Surface aerosol concentrations are measured mainly through two instruments, the CCNPC and CPC onboard the Horizon Lines cargo ship. The N_{CCN} values were measured by CCNPC at supersaturation (SS) levels of 0.0%, 0.1%, 0.2%, 0.3%, 0.4%, and 0.6% over 10 min, respectively, during MAGIC. Thus, we normally use the 10-min averages at each SS to represent each hour of N_{CCN} information at a specific SS. In this study, we use the N_{CCN} values at SS = 0.2% as a representative CCN because N_{CCN} at 0.2% supersaturation represents the typical condition of MBL clouds (Dong et al., 2014). During MAGIC, we found that the retrieved MBL cloud-droplet number concentration (N_C) has the highest correlation with the N_{CCN} at SS = 0.2%. For example, the correlation coefficients between surface N_{CCN} to retrieved N_C are 0.10, 0.20, 0.25, 0.22, 0.16, 0.15 for 0.0%, 0.1%, 0.2%, 0.3%, 0.4%, and 0.6% SS, respectively, during MAGIC.

The surface CN concentrations (N_{CN}) were measured simultaneously with a range of aerosol particle sizes from 10 to 3,000 nm. Temporal resolutions were at 1 s for both CPC and CCNPC measurements. Because CPC measurements encompass measurements by CCNPC, ratios for the number of aerosols that become activated at the given supersaturation can be further investigated. To avoid the impacts of pollution on the aerosol measurements, the CPC and CCNPC instruments were located away from the ship's exhaust plumes. However, sudden spikes of N_{CN} and N_{CNN} were still observed during MAGIC operation during sudden changes in wind direction. Painemal et al. (2015) analyzed these spikes and concluded that they are most likely emissions from nearby ships or other onboard emissions based on the small diameters of these aerosol particles. In this study, we adopt the method used in Painemal et al. (2015), namely, standard deviations of N_{CN} and N_{CCN} for each hour were calculated; the periods when deviations were greater than 100 cm^{-3} were removed to eliminate these spikes.

The University of Wisconsin vertical pointing HSRL (Eloranta, 2005) provided the profiles of particle backscatter cross-section, extinction, and optical depth throughout the atmospheric column during MAGIC. To retrieve the N_{CCN} profile below cloud base, particle backscatter cross-section is used in this study because it is not strongly affected by calibration issues and signal noise. The uncertainty of the HSRL measured particle backscatter cross-section is approximately 0.36/Mm sr (Su et al., 2008). The HSRL operated at a wavelength of 532 nm with a temporal resolution of 30 s and a vertical resolution of 30 m. Although HSRL can measure aerosols, hydrometers, and cloud droplets, its signals can be severely attenuated by cloud droplets, especially for drizzling clouds. To provide an accurate estimate of the N_{CCN} profile from HSRL measurements, the Ka ARM Zenith Radar (KAZR) and laser ceilometer measurements were used to provide the MBL cloud and drizzle information, as well as cloud base height. Because the HSRL wasn't operating at the beginning of the MAGIC field campaign, only the measurements during warm-season months (May–September) are used in this study.

Balloon radiosondes were launched approximately every 6 hr during the ship legs of MAGIC, which provided vertical profiles of atmospheric temperature, relative humidity, and winds. These profiles are used to determine continuous atmospheric profiles to calculate the humidification factor required in the aerosol retrieval algorithm in this study. Based on the ratio from the last and next sounding distances, a continuous atmospheric profile can be interpreted for a portion of each leg. These continuous atmospheric profiles are further used to classify boundary layer conditions as coupled or decoupled. To be classified as coupled, the boundary layer must be well mixed where the potential temperature, θ, and mixing ratio are nearly constant with height from the surface to cloud base. Taking the difference of θ between cloud base and the surface, a threshold of $\Delta\theta < 0.5$ K is used to define whether the boundary layer is coupled (Dong et al., 2015; Jones et al., 2011). Typically, over the MAGIC

transect, the boundary layer is initially coupled just off the coast of LA; as sea surface temperatures (SSTs) warm moving westward, conditions switch to being decoupled with the location of this switch varying (Bretherton & Wyant, 1997; Wyant et al., 1997; Zhou et al., 2015).

2.2. Retrieval Methods

Proposed in Ghan and Collins (2004) and Ghan et al. (2006), the retrieval methods used in this study allow for the estimation of N_{CCN} with height. Ghan et al. (2006) found the retrieval is more accurate for supersaturations at/near 0.1% than for supersaturations greater than 1.0%, as these particles have a greater influence on backscatter/extinction. As described in Ghan and Collins (2004) and Ghan et al. (2006), a few assumptions were used in this retrieval method. For example, the aerosol size distribution and composition were assumed constant with height. It is expected that these assumptions are more likely to be valid for a coupled boundary layer because the aerosols are vertically well mixed, which enhances the feasibility of the retrieved N_{CCN} profile (Dong et al., 2015). A more detailed description of the retrieval methods can be found in Ghan and Collins (2004) and Ghan et al. (2006).

Because the backscatter by aerosols is dependent on the relative humidity, the humidification factor must be considered (Gasso et al., 2000). While Equation 1 was developed in the Atlantic, it was confirmed for MAGIC using limited nephelometer data in Painemal et al. (2017).

$$f(RH) = 0.76 \cdot \left(1 - \frac{RH}{100}\right)^{-0.69} \tag{1}$$

Using the interpreted relative humidity profiles to determine this factor, the dry backscatter signal, $\sigma_d(z)$, can then be obtained using Equation 2 as follows

$$\sigma_d(z) = \sigma(z)/f(RH, z) \tag{2}$$

The threshold of $f(RH, z)$ is approximately 1 at $RH = 40\%$. When RH values are lower than 40%, $f(RH, z)$ remains between 0.75 and 1, $\sigma_d(z)$ values are greater than the HSRL measured $\sigma(z)$. When RH values are greater than 40%, $f(RH, z)$ increases to ~4 at $RH = 90\%$, thus $\sigma_d(z)$ values are ~25% of the HSRL measured $\sigma(z)$. Thereafter, $f(RH, z)$ exponentially increases to infinity as RH approaches 100%. Because of this, locations where RH exceeds 95% are removed from the retrieval to reduce error. Based on $\sigma_d(z)$ from Equation 2 and surface measured N_{CCN}, a vertical profile, $N_{CCN}(z)$, can be estimated using a simple ratio in Equation 3

$$N_{CCN}(z) = N_{CCN}\frac{\sigma_d(z)}{\sigma_d(0)} \tag{3}$$

In this study, we assume the lowest (150 m) particle backscatter cross section, $\sigma_d(0)$, measured by the HSRL, is the same at the surface measurement σ_{sfc}, then a ratio can be applied based on the surface measured N_{CCN} to provide an estimate of the N_{CCN} profile using Equation 3. The validity of this assumption [$\sigma(0) \sim \sigma_{sfc}$] will be discussed as follow. Though this assumption is hard to validate in this study mainly due to the lack of in-situ aerosol measurements made above the ship, we provide a few pieces of evidence to partially prove the validity of this assumption. Schulze et al. (2020) analyzed aerosol profiles from aircraft measurements off the coast of California and found that CN and CCN concentrations were mostly constant from ~50 through ~200 m. Although these measurements can partially answer this question, there were no in situ measurements below 50 m due to safety issues. However, this assumption may never be validated because the ship-based instruments and aircraft in situ probes cannot measure aerosol concentrations between the ocean surface and an altitude of 50 m.

To further explore the validity of this assumption, we investigate the variations of surface wind speed and try to find any correlations between the wind speeds and the retrieved N_{CCN} results and backscatter measurements during MAGIC. Monahan et al. (1983) found that strong winds producing white capping conditions (occurring at wind speed > ~10 m/s) can lead to large increases in surface aerosols (<50 m). Based on this conclusion and available measurements during MAGIC, we first looked at the surface backscatter measured by the Nephelometer against the lowest HSRL gate backscatter (150 m) to see if there is any correlation between the two measurements. Because these instruments measure backscatter differently, they give different units which aren't easily convertible. Figure S1 in Supporting Information S1, shows a scatterplot between two matched measurements. Overall, they have fairly a good correlation with a coefficient of 0.67. While this comparison doesn't mean that

the aerosol concentrations at these two layers (Ocean surface and an altitude of 150 m) are the same, it does help to prove that there is favorable mixing between the two layers.

To further investigate the relationships between the surface wind speed and two measurements at the ocean surface and an altitude of 150, we plot Figure S2 in Supporting Information S1 using the data collected during MAGIC. Both measurements show a similar relationship with almost the same correlation coefficient with the surface wind speed. As expected, the measured backscatter values from the two instruments increase with increased wind speed due to increased sea spray. Since the relationship is similar to each other in these two levels, it is hard to believe that there are large variations in aerosol concentration in these two levels. However, we cannot rule out this possibility for higher wind speeds. As demonstrated in Figure S2 in Supporting Information S1, most of the 5-min averaged wind speeds are less than 12 m/s because our data sets were collected during the warm months where synoptic events are typically weaker, wind speed stays relatively light to hinder white capping conditions.

Moreover, we investigated the relationships between cloud-droplet number concentration (N_c) and surface N_{CCN} under the conditions when the surface wind speeds were greater and less than one standard deviation from the mean surface wind speed. As illustrated in Figure S3 in Supporting Information S1, both relationships and correlations (N_c vs. $N_{CCN0.2}$) are similar to each other. The CCN concentrations in Figure S3b in Supporting Information S1 are indeed higher than those in Figure S3a in Supporting Information S1, indicating that the surface CCN concentrations increase with increased surface wind speed. This conclusion was also proved from other studies (e.g., Dong et al., 2014; Logan et al., 2014). However, the ACI and correlation in Figure S3b in Supporting Information S1 are nearly identical to those in Figure S3a in Supporting Information S1, suggesting that there are no significant changes in ACI and correlation under both conditions. The figures and the findings shown support our assumption that the CCN concentrations at the surface are similar to those at an altitude of 150 m.

3. Results and Discussions

3.1. In Situ Measurements

Figure 1 shows the probability density functions (PDFs) for both N_{CCN} at 0.2% SS ($N_{CCN,0.2}$, left) and N_{CN} (right) during the MAGIC field campaign with the means of $N_{CCN,0.2}$ and N_{CN} of 116.7 cm^{-3} and 219.4 cm^{-3}, and standard deviations of 80.4 and 153.8, respectively. Above each PDF is a boxplot for the corresponding data showing minimum, 25th percentile, median, 75th percentile, and maximum where the medians of $N_{CCN,0.2}$ and N_{CN} are 97.9 and 189.7 cm^{-3}, respectively. Both PDFs show a positively skewed distribution, leading to mean values to be ~15% higher than medians. The mean ratio of $N_{CCN,0.2}$ to N_{CN} is 52.4%, indicating that more than half of CN particles were converted to CCN during MAGIC at 0.2% SS. To better represent marine aerosol environments, observations within ship docking stations were excluded from this data set.

As discussed in Painemal et al. (2015), MAGIC did show strong seasonal variability in aerosol concentrations, with the maximum values occurring during the summer months. Stronger easterly winds due to summer subtropical high-pressure systems are likely attributed to this seasonal variation. While the seasonal variability is important, knowing how aerosol concentrations change heading toward HI also remains vital and is a focus of this study. Figure 2 shows boxplots of the longitude variation of $N_{CCN,0.2}$ (Figure 2a) and N_{CN} (Figure 2b) during the entire MAGIC field campaign with LA on the right and HI on the left. Starting on the right near LA, each boxplot represents the 2-degree longitude averages. As illustrated in Figure 2, the highest concentrations and variations occurred near LA for both $N_{CCN,0.2}$ and N_{CN} due to anthropogenic and continental sources being advected into this region. Westward of LA, both $N_{CCN,0.2}$ and N_{CN} decreased monotonically with three stages. From LA to ~−130° longitude, mean N_{CN} drop from ~600 to ~260 cm^{-3}, and mean $N_{CCN,0.2}$ from ~300 to ~150 cm^{-3}, that is, both $N_{CCN,0.2}$ and N_{CN} decreased more than half. From −140° to −130° longitude, mean N_{CN} declined gradually from ~260 to ~200 cm^{-3}, and mean $N_{CCN,0.2}$ from ~150 to ~100 cm^{-3}. From −140° longitude to HI, mean $N_{CCN,0.2}$ and N_{CN} remained steady just over 100 cm^{-3} and 200 cm^{-3}, respectively. Figure 2c shows the ratios of N_{CN} to $N_{CCN,0.2}$ over the same distance where the ratios slightly decreased westward, mostly close to or below two, indicating that more than half of the N_{CN} become activated at 0.2% SS and the ratios do not vary significantly over ENP. Small variations at each boxplot indicate slight changes in this ratio over ENP except for relative higher values with larger variation near LA due to smaller-sized, recently formed particles. Note that a similar trend was also found in latitude (not shown).

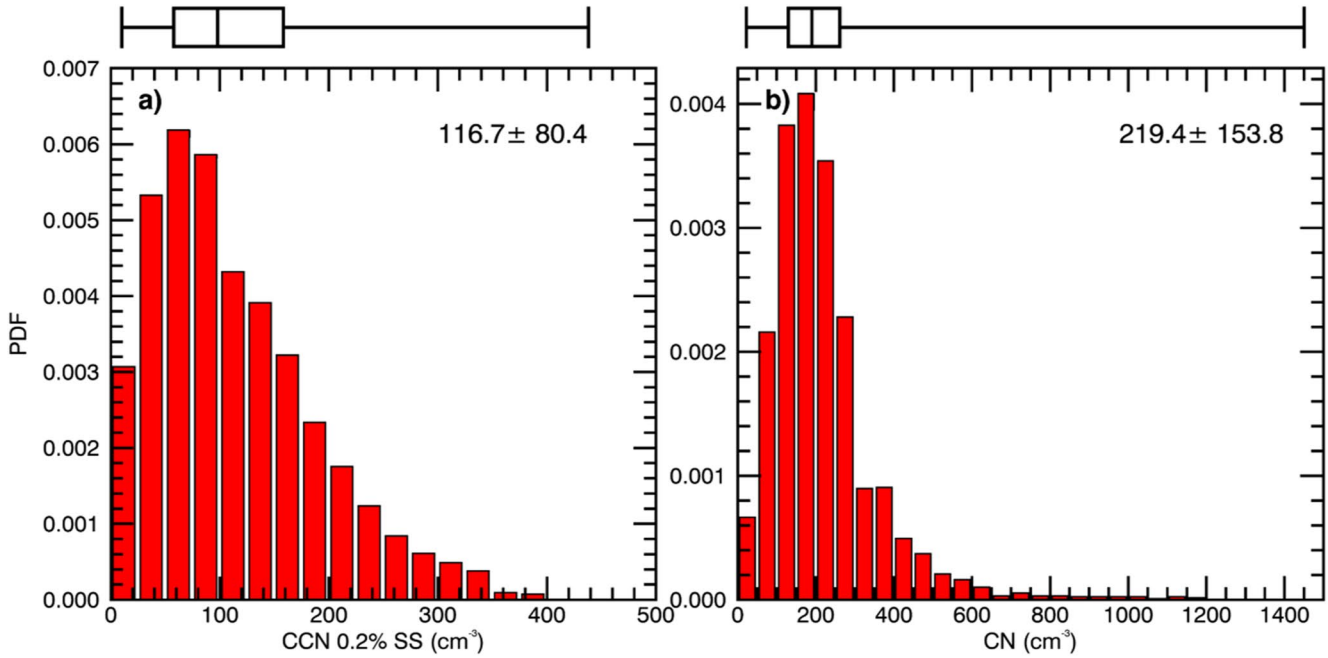

Figure 1. Probability density functions (PDFs) of (a) Cloud Condensation Nuclei (CCN) concentration at 0.2% supersaturation ($N_{CCN,0.2}$) measured by CCN Particle Counter (CCNPC) and (b) Condensation Nuclei (CN) concentration (N_{CN}) measured by Condensation Particle Counter (CPC) over the Eastern North Pacific (ENP) during MAGIC (October 2012–September 2013). Means and standard deviations are labeled inside the PDFs. Above this, is the corresponding boxplot showing minimum, 25th percentile, medium, 75th percentile, and maximum. The MAGIC field campaign is a ship-based experiment between Los Angles (−118° E longitude) and Honolulu (−158° E longitude).

3.2. Retrieved CCN Profile

Using the methods discussed in Ghan and Collins (2004) and Ghan et al. (2006), N_{CCN} profiles were retrieved when all measurements were available during the MAGIC field campaign. Averages were calculated over 10-min intervals corresponding to the times when $N_{CCN,0.2}$ was measured. Since six different supersaturations were measured over an hour, only one measurement per hour was calculated. Thus, a total of 1,295 N_{CCN} profiles were retrieved during May–September 2013 when HSRL data was available. Because the HSRL observations are severely attenuated by cloud and drizzle droplets, these attenuated signals were removed and not used in the retrieval. The periods for performing N_{CCN} retrievals include no clouds, non-drizzling MBL clouds, and clouds producing virga (i.e., drizzle evaporating before reaching the surface). These conditions were determined based on cloud and drizzle retrieval outputs in Brendecke et al. (2021). Among the 1,295 retrieved N_{CCN} profiles, 325 cases (25.1%) are for clear-sky conditions (no clouds), 556 cases (42.9%) for non-drizzling clouds, and 414 cases (32.0%) for virga. For both cloud and virga cases, N_{CCN} profiles were retrieved from the surface to cloud base.

Figure 3 shows a sample case for the retrieval inputs along with the output of $N_{CCN,0.2}$ profiles for a portion of Leg 15A (20–24 July 2013). This leg represents a classic SCT case as observed by KAZR reflectivity in Figure 3a with ceilometer detected cloud base (black dots). Starting from the right side of Figure 3a, more stratocumulus clouds and drizzle occurred near LA (∼−120°E), then followed by virga and drizzle with increasing cloud height until around −138°E. Hereafter, the cloud regime transitions to a cumulus dominant cloud type with periods of brief but heavy drizzle. In Figure 3b, interpreted relatively humidity based on soundings over the same period is shown. Relative humidity increases gradually from the surface to the cloud base, and the maximum relative humidity variation mimics the longitudinal variation of cloud-base height, increasing from LA to the cloud breakup (CB) near −138°E. Compared to eastward of the CB, relative humidity near the CB is lower. After the CB (westward), the boundary layer becomes decoupled with two peaks of high humidity near 0.75 km and just below 2.0 km (Bretherton & Wyant, 1997; Wyant et al., 1997).

Hourly averaged surface humidification factor, f(RH, z), is calculated from Equation 1 based on the continuous RH profiles in Figure 3b. Figure 3c shows the f(RH, z) values which mimic the variations of RH profiles in Figure 3b with an overall average of 1.71. Hourly surface $N_{CCN,0.2}$ values measured by CCNPC are shown in

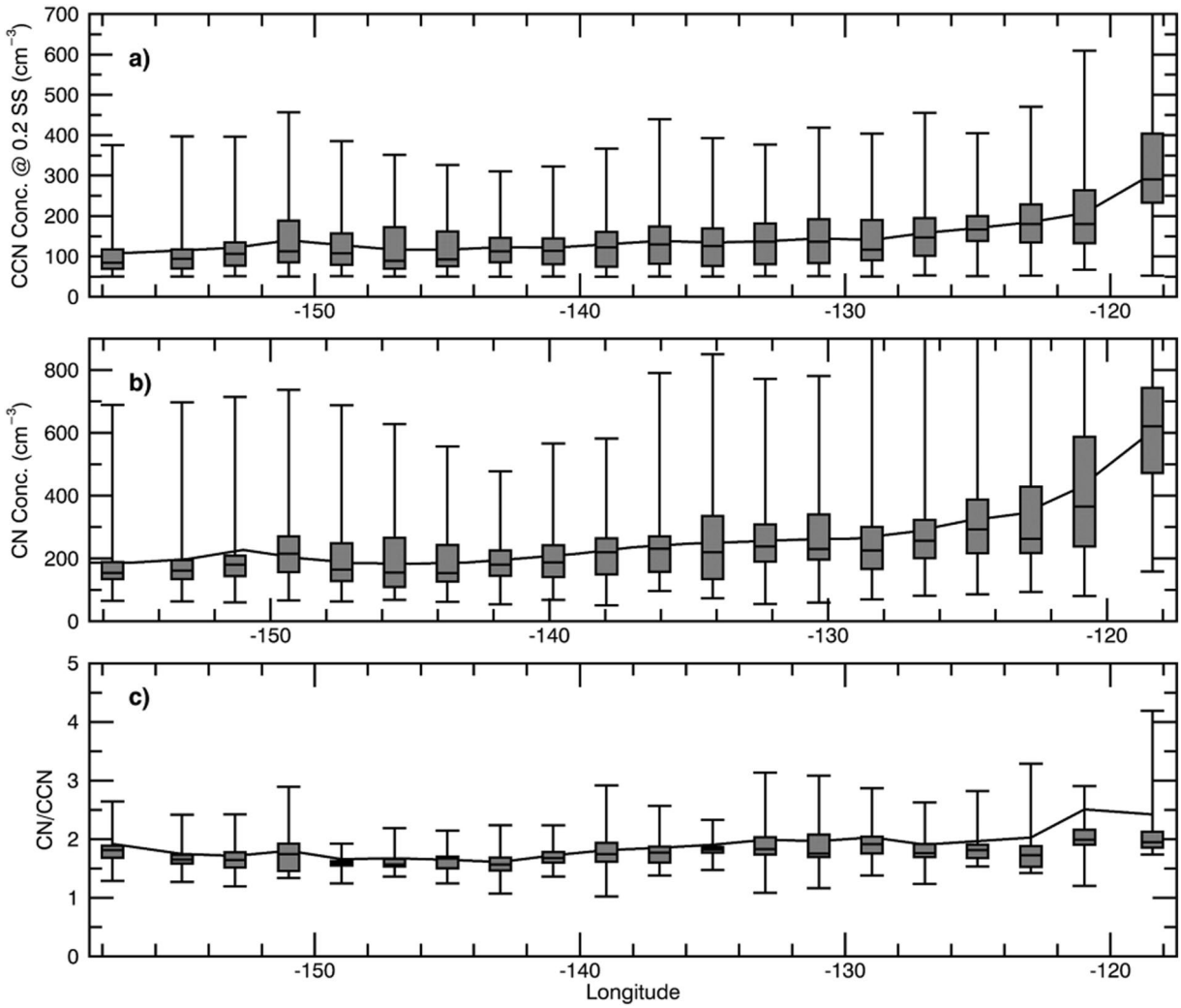

Figure 2. (a) Longitude variations of $N_{CCN,0.2}$ from Honolulu (−158° E) to Los Angles (−118° E) with each boxplot representing averaged 2° longitude interval during the MAGIC field campaign. Continuous lines represent mean values over the same region. (b) Same as (a) but for N_{CN}. (c) Ratio of N_{CN} to N_{CCN} in (a) and (b).

Figure 3d with the highest concentration of ∼250 cm^{-3} near LA, reaching the lowest concentration of ∼100 cm^{-3} at −125°E, then bottoming out and gradually climbing up to ∼250 cm^{-3} near −145°E. Further explanation about aerosol variations over the SCT will be given in Section 3.4. Shown in Figure 3e, 5-min averaged particle attenuated backscatter measurements from HSRL below the cloud base are plotted, where the measurements collocated with drizzle and cloud identified by Ka-band radar (Figure 3a) are removed. Adjusting the HSRL measured backscatter measurements to the dry backscatter using Equation 2 will allow us to estimate $N_{CCN,0.2}$ profiles using in Equation 3. As presented in Figure 3f, the strongest backscatter regions were removed due to interpreted relative humidity profiles not being able to capture details between soundings. In general, the retrieved CCN concentrations decrease with height during this leg.

To provide statistical results of N_{CCN} profiles over ENP, normalized N_{CCN} profiles from the surface to cloud base (970 samples) are selected to better understand the relationship between N_{CCN} profiles with the surface N_{CCN} and cloud-droplet number concentration (N_C). As mentioned above, most previous studies used the surface measured N_{CCN} as a proxy to investigate ACIs (e.g., Dong et al., 2015) because they all assumed the surface measured N_{CCN} to be comparable to that below the cloud base. Theoretically, the aerosols just below the cloud base (not at the surface) are supposed to be used for studying more direct interactions between aerosols and cloud microphysical properties.

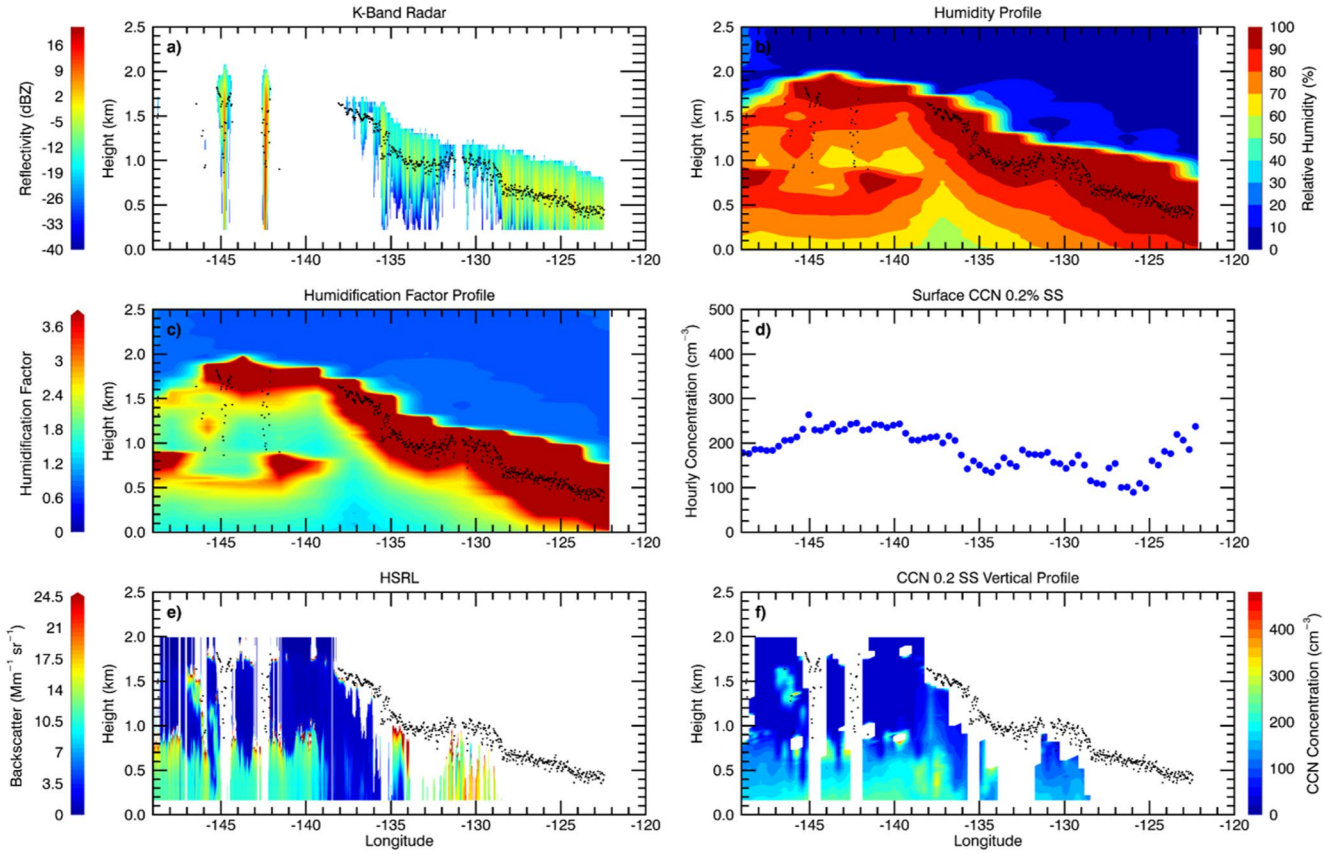

Figure 3. The surface-based radar-lidar observations and retrieved $N_{CCN,0.2}$ profiles during the MAGIC Leg 15A (20130720–20130724). (a) Reflectivity profiles measured by Ka-band zenith pointing radar. Black dots represent the cloud bases derived from laser ceilometer. (b) Relative humidity profiles interpolated from balloon sounds. (c) Hourly mean humidification factor, $f(RH)$, derived from (b). (d) Hourly mean surface $N_{CCN,0.2}$ measured onboard the ship. (e) 5-min averaged particle backscatter cross section measurements by High Spectral Resolution Lidar (HSRL) below the cloud base. Note that the HSRL measurements are attenuated by drizzle and removed. (f) Retrieved $N_{CCN,0.2}$ profiles below the cloud base from the measurements of surface $N_{CCN,0.2}$ and dry backscatter profiles.

Figure 4 shows the normalized $N_{CCN,0.2}$ profiles during MAGIC where 0.0 represents the surface and 1.0 at the cloud base. Furthermore, the boundary layer conditions are classified as decoupled (blue) and coupled (red) based on the definition of Jones et al. (2011) and Dong et al. (2015). Figure 4a shows the mean normalized profiles of $N_{CCN,0.2}$ for both coupled and decoupled boundary conditions. Note that the time periods without clouds (325 samples) were not included in this analysis in order to investigate the relationships between $N_{CCN,0.2}$ and N_C. Shaded regions represent one standard deviation with the associated colors. A total of 250 profiles were identified for coupled and 720 for decoupled conditions. Decoupled CCN concentrations decrease by ∼25 cm^{-3} (∼20%) from the surface to cloud base. Whereas the coupled CCN concentrations decrease by ∼20 cm^{-3} (∼14%) and show higher concentrations than the decoupled values. The higher $N_{CCN,0.2}$ and less decrease from the surface to cloud base during coupled conditions make physical sense and are consistent with previous studies (e.g., Dong et al., 2015).

The profiles of correlation coefficients between the retrieved N_{CCN} profiles with the CCNPC measured $N_{CCN,0.2}$ at the surface are shown in Figure 4b. As expected, both the correlation coefficients for coupled and decoupled conditions from the surface to the near middle (Normalized Height ∼0.45) are nearly perfect ($R > 0.9$) with almost 1 near the surface. This is understandable because the CCNPC measured $N_{CCN,0.2}$ at the surface is used as a constraint in the retrieved N_{CCN} profile as well as aerosols being well-mixed in this layer. The correlation coefficients for coupled conditions remain high (R ∼ 0.9) between the middle to cloud base. However, for decoupled conditions, the correlation coefficients decrease from 0.9 to 0.8, presumably due to the loosed connection between surface aerosols and the atmospheric boundary layer. The correlation coefficients in Figure 4b have demonstrated that the previous assumptions are mostly valid for coupled conditions, while it should be used with caution for decoupled conditions. However, depending on where the MBL inversion layer is trapping the

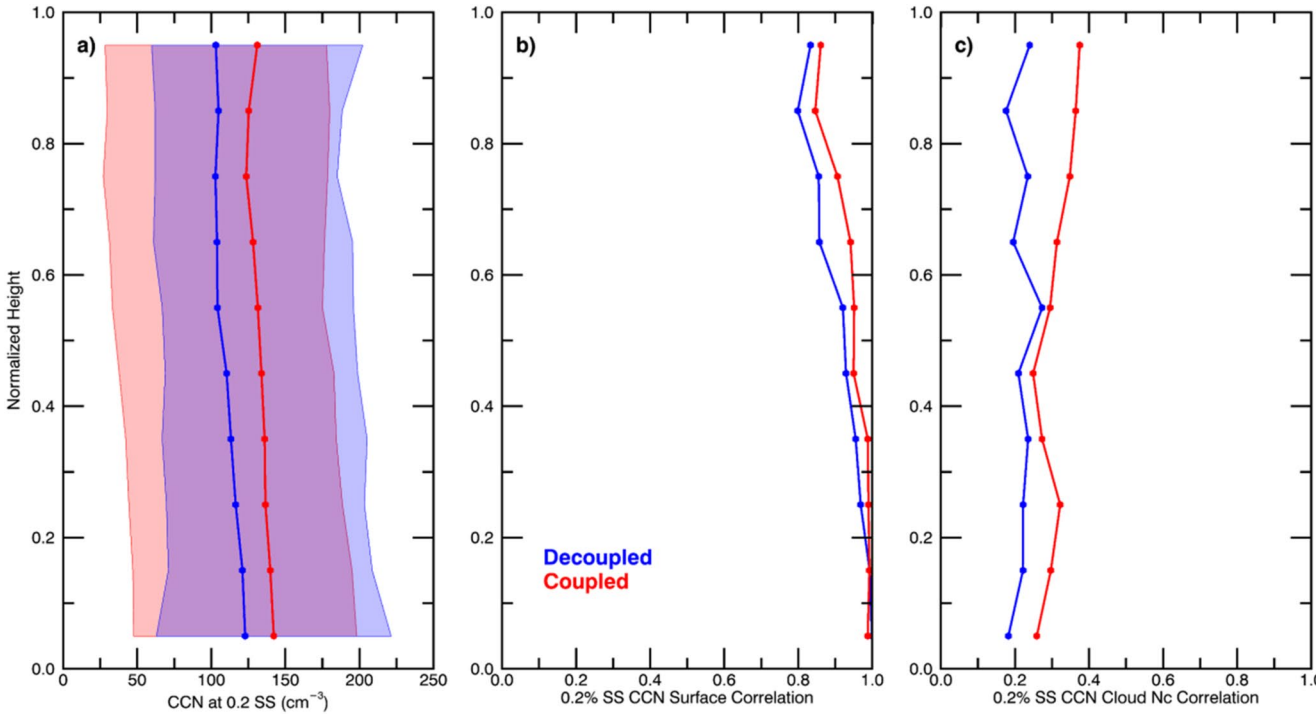

Figure 4. (a) Normalized mean $N_{CCN,0.2}$ from the surface to the cloud base for coupled (red) and decoupled (blue) boundary layers. Shaded areas represent one standard deviation. Profiles of the correlation coefficients between the HSRL-retrieved $N_{CCN,0.2}$ profiles with (b) the surface measured $N_{CCN,0.2}$, and (c) cloud-droplet number concentration (N_c) presented in Brendecke et al. (2021).

near-surface moisture and aerosol, even under the decoupled condition, it is still feasible to use the N_{CCN} retrieval below the boundary layer inversion height, as this layer is often well-mixed and driven by the surface fluxes.

Likewise, Figure 4c shows the profiles of the correlation coefficients between the retrieved N_{CCN} profiles with the retrieved N_c where N_c values were presented in Brendecke et al. (2021) and averaged over the corresponding 10-min interval. The cloud and drizzle microphysics retrieval methods were developed in Wu et al. (2020) using radar, ceilometer, and microwave radiometer and assumes a constant N_C with height. This allows for a simple calculation of the correlation coefficient. As explained earlier, aerosol concentrations are expected to have a positive correlation with N_C with a higher correlation occurring just below the cloud base where aerosols become activated as CCN. This is particularly true for coupled conditions where the correlation coefficients increase from 0.25 near the surface to 0.4 just below 0.4. For decoupled conditions, the average correlation coefficient stays near constant around 0.20 and with height. The higher correlation coefficients near the cloud base for coupled conditions are reasonable and what we expected. Note that Painemal et al. (2017) found that the correlation coefficient can be up to 0.7 using the satellite retrieved N_C and surface measured N_{CCN}. The lower correlation coefficients in this study may be due to different retrieval methods in N_C and N_{CCN} profile between two studies and the fixed supersaturation used in this study.

To investigate the correlation variation with height, Figure 5 shows scatterplots of N_C versus $N_{CCN,0.2}$ below the cloud base (Normalized Height = 0.95) in Figure 5a and near the surface (Normalized Height = 0.05) in Figure 5b for coupled conditions. Also show is the correlation coefficient. As illustrated in Figure 4c, the correlations increase by 0.12 (46.2%) from the surface to the cloud base which is demonstrated in Figure 5. While correlation values are lower than what we expected, the increased percentage is encouraging. That is, the N_{CCN} values near the cloud base should be used to study ACIs, which should be more representative than using surface N_{CCN}. Better understanding the magnitude of this change will allow future studies to better quantify their results when comparing surface aerosols to cloud properties.

Similar to Figure 4, Figure 6 decomposes the coupled conditions into two categories based on their precipitation status, namely non-drizzling (red) and virga (blue) clouds. A total of 157 cases were used for non-drizzling and 93 cases for virga. Similar to Figure 4a, the normalized mean $N_{CCN,0.2}$ profiles from the surface to the cloud

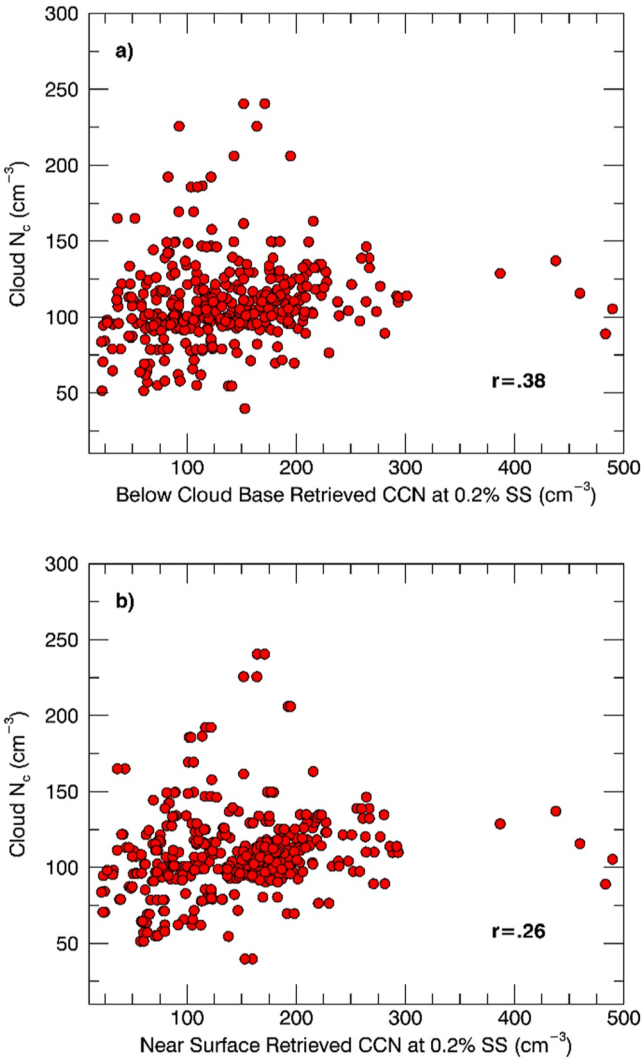

Figure 5. Scatterplots of N_c versus the retrieved $N_{CCN,0.2}$ of (a) just below the cloud base and (b) just above the surface based on selected normalized heights for coupled boundary conditions shown in Figure 4.

base for both non-drizzling (red) and virga clouds (blue) are almost identical to the N_{CCN} profile under the coupled condition. Note that the samples for virga decrease with height and no values just below cloud base due to signal attenuation. Compared with surface N_{CCN} measurements in Figure 6b, both non-drizzling and virga cases show nearly the same correlation with height, both decreasing by ~0.10. Compared with N_c, the correlation coefficients for non-drizzling clouds are much higher than those for virga, increasing from 0.35 at the surface to 0.45 near cloud base. For virga samples, however, their correlation coefficients are close to 0.2 for most of the layer, which is almost identical to those of decoupled cases. Precipitation scavenging could be a major reason for the differences between these two conditions. As hydrometers fall, they intercept aerosols to alter aerosol concentrations and decrease correlation with N_C, this argument could be proven by the decreased correlation coefficients with height, especially near the cloud base. It should also be noted that while hours dominated by drizzling clouds (drizzle reaching the surface) cannot be used in the retrieval, a lower correlation coefficient would be expected due to increased wet scavenging.

3.3. Estimation of Retrieved N_{CCN} Uncertainty

Before knowing the retrieved N_{CCN} uncertainty, the uncertainties from the retrieval inputs must first be known. As mentioned above, uncertainty from the HSRL backscatter cross section is estimated to be ±0.36 Mm sr^{-1} (Su et al., 2008). Errors by the CCNPC is estimated to be 11% (Painemal et al., 2017) on average. As discussed in Section 2.2, further uncertainties come from $f(RH, z)$ as $RH(z)$ is interpolated from balloon soundings and isn't measured continuously. Comparing surface interpolated RH with continuously measured RH from meteorological instrumentation onboard the ship gives $f(RH, z)$ an uncertainty of ±0.64, as $RH(z)$ is rarely under 50% below cloud base and values above 95% are excluded. This uncertainty is assumed to be true for all heights. Based on these errors, a calculated error of ±12.5 cm^{-3} is estimated for retrieved N_{CCN} profiles. This retrieval uncertainty is estimated theoretically by propagating observational errors through the retrievals. While this method is used to estimate the retrieval uncertainty, it fails to quantify the uncertainties from different assumptions made within the retrieval. Hence, a further assessment using the aircraft in situ measurements of N_{CCN} is guaranteed in future work.

3.4. The Relationship Between Aerosol and SCT

Another critical goal of the MAGIC campaign was to better understand the factors leading to CB and the transition from stratocumulus (Sc) to cumulus (Cu) cloud regime. Bretherton and Wyant (1997) and Wyant et al. (1997) proposed a commonly accepted but simple theoretical model for understanding the SCT, in which the advection of cloud systems from Sc to Cu over an increasing SST allows for more favor to generate decoupled conditions. The SCT separates the MBL into a Cu favored surface flux driven convection and a Sc favored longwave radiative cooling convection. As rising Cu become more vigorous with increasing SST, they can penetrate the stable layer into the cloud-top inversion layer. Much drier air is typically observed above this cloud-top inversion (Bretherton et al., 2010) leading to entrainment of dry air and the decline of Sc coverage. Furthermore, the dynamic forcings were found to be an important factor in generating the SCT during the MAGIC field campaign with Zhou et al. (2015) identifying that high pressure systems typically occurred eastward of CB.

While dynamic forcings ultimately dictate the SCT, drizzle should also be considered an important factor in this transition (Yamaguchi et al., 2017). Therefore, it is necessary to investigate how aerosol concentrations change before, during, and after CB, and if these changes are associated with drizzle or other factors. Seven SCT events (Legs 7B, 11A, 14B, 15A, 15B, 16A, and 18B) are selected and their surface CN concentrations, surface wind

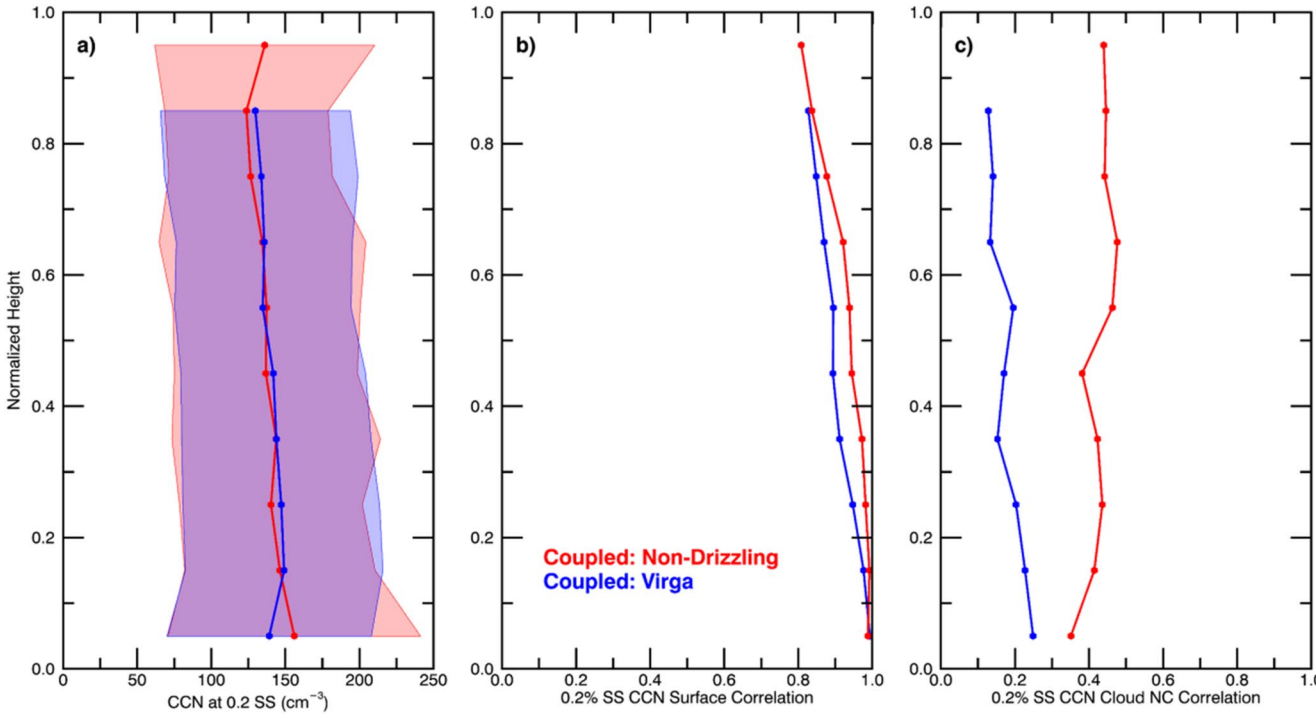

Figure 6. Same as in Figure 4 but for Coupled Non-Drizzling (red) and Coupled Virga (blue) cases.

speeds, and cloud fractions (CFs) are plotted in Figure 7. These results have clearly demonstrated that there are sudden changes in CN concentration, wind speed, and CF near CB.

Figure 7a shows the N_{CN} differences from Leg mean N_{CN} before (stratocumulus regime), during, and after (cumulus regime) CB, averaged over the seven cases. Averages are taken 8° before and after CB with points representing a 0.8° longitude average; standard deviation is shown in the shaded region. Before CB, closer to LA, N_{CN} decreases ∼75 cm^{-3} as the ship moves farther west from continental aerosol sources. A minimum N_{CN} occurs surrounding CB and then gradually increases ∼25 cm^{-3} near 3°W of CB within the cumulus cloud regime. Thereafter, CN concentrations continue to increase gradually but remain steady around the leg mean. Figure 7b shows the surface wind speeds over the same region measured onboard by the Marine Surface Meteorological Instrumentation. Overall, the surface wind speeds gradually increase from ∼5 m s^{-1} near far east to ∼7 m s^{-1} near far west with a distinguishable increase during CB.

Cloud fractions determined by ARM radar-lidar observations are shown in Figure 7c for these seven selected cases. Contrasting to its surface wind counterpart, CF generally decreases westward with relatively large variation. As expected, more clouds occur before CB with the highest CF near 90% about 4°E of CB. This region would also be associated with strongly drizzling clouds which could attribute to the decreased N_{CN} values before CB. Based on the results in Figure 7, we can tentatively draw a conclusion. The decreased N_{CN} trend over the east of CB is mainly caused by Sc precipitation scavenging, while the increased N_{CN} trend west of CB is strongly associated with the increased surface wind speed and fewer drizzle events. While wind speed still increases east of CB, precipitation scavenging and decreasing aerosols west of LA (shown in Figure 2) dominate the aerosols concentration, decreasing $N_{CCN,0.2}$ and N_{CN} east of CB. After CB these two factors diminish to allow wind speed as the dominating factor controlling aerosol concentrations. The only drawback of this conclusion is limited by the ship-based measurements, which may motivate more measurements and model simulations to further investigate this process in the future.

Figure 8 shows the changes in $N_{CCN,0.2}$ profiles for before (stratocumulus regime), during, and after (cumulus regime) CB. Due to limited retrieval coverage, only three Legs (14B, 15A, and 18B) are selected to have complete $N_{CCN,0.2}$ profiles before, during, and after CB in Figure 8. A 2° longitude average was taken during the transition as well as a 2° longitude average 1°–3° east and west of the breakup. Normalized heights are again

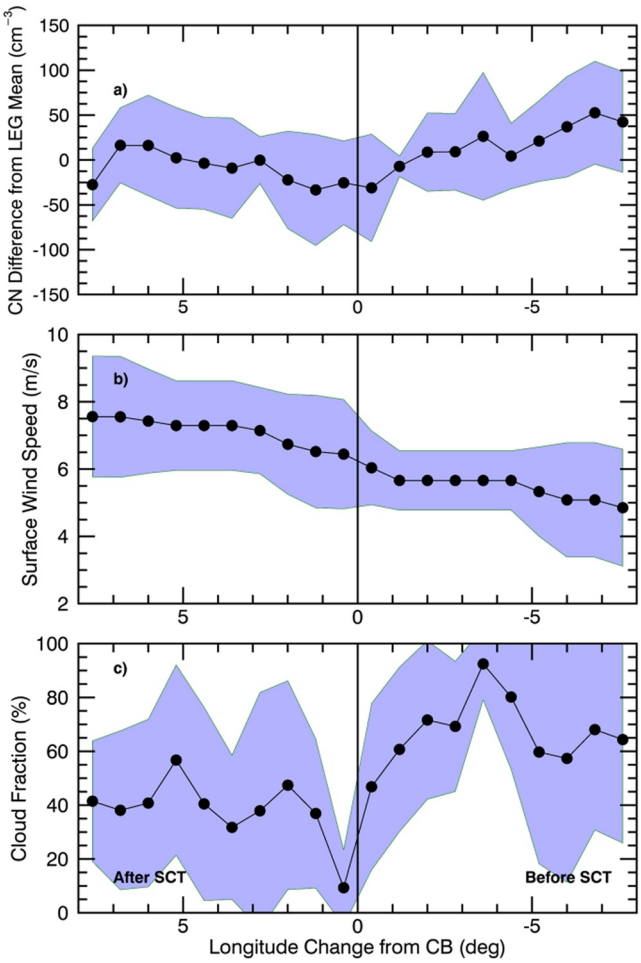

Figure 7. Composite changes in aerosol and meteorological conditions over the stratocumulus to cumulus transition (SCT) from seven selected Legs during MAGIC. Each point represents a 0.8 longitude averaging with the centerline representing the cloud breakup (CB). Shaded regions represent one standard deviation. Legs 7B, 11A, 14B, 15A, 15B, 16A, and 18B were selected and averaged together. (a) N_{CN} difference from Leg means and N_{CN} measured by CPC, (b) mean surface wind speed measured from Marine Surface Meteorological Instrumentation, and (c) cloud fraction determined by KAZR reflectivity.

used to show the changes in $N_{CCN,0.2}$ profiles with shaded areas representing one standard deviation. All cases show a decreasing trend in $N_{CCN,0.2}$ with height but more importantly, a minimum is seen during CB. Layer averages are 144.9, 91.4, and 161.2 cm^{-3} for before, during, and after, respectively, with the largest variance occurring after the SCT. These results are consistent with those in Figure 7. However, it is a challenge to tell that the minima CN and CCN concentrations during CB are causes or effects of the SCT. A further study is needed using high-resolution models to simulate these events.

While it is a well-known fact that dynamic forcings play an important role in CB, the role of environmental conditions and their impacts on surface aerosols could not be ignored as demonstrated in Figures 7 and 8. As illustrated in Figure 3b, lower relative humidity is observed near CB centered at −137°E, so do for the legs 14B and 18B. Additionally, increased wind speeds after CB are observed as shown in Figure 7b. Both relative humidity and surface wind speed suggest that changes in air masses are likely linked to CB, but they are more likely the effects of CB, not triggering CB (dynamic forcings). These results are consistent with the findings in Zhou et al. (2015). Because decoupling happens over the east of CB found in this study and in Zhou et al. (2015), moisture supply is typically cut off near or before CB. Both drizzle and water vapor cut-off help lead to CB. After CB (west), an increase in aerosols is most likely resulted from increased surface wind speeds due to changes in air masses. As surface wind speed increases, sea spray is more likely to be picked up and evaporated into the air, attributing to increased aerosol concentrations.

4. Summary and Conclusion

Maritime aerosol and cloud measurements and retrievals taken during the MAGIC field campaign provide a great opportunity to investigate the longitudinal (as well as latitudinal, not shown) variations of aerosol and cloud properties, as well as their interactions, over the Eastern North Pacific (ENP). The retrieved N_{CCN} profiles can help to further reveal the assumption used in most previous studies, that is, the surface measured N_{CCN} is comparable to that below the cloud base. Finally, the causes and effects of the SCT, as well as the N_{CN} variations before, during, and after SCT are investigated in this study. Based on the ship-based aerosol and cloud observations and retrievals during MAGIC, we report the following summary and conclusions:

1. During MAGIC, the ship-based in-situ measured $N_{CCN,0.2}$ and N_{CN} had mean values of 116.7 and 219.4 cm^{-3} with standard deviations of 80.4 and 153.8 cm^{-3}, respectively. The highest concentrations were found closest to LA due to an increase in aerosol sources. Moving westward, both CN and CCN concentrations gradually decrease until stabilizing near 100 cm^{-3} for $N_{CCN,0.2}$ and 200 cm^{-3} for N_{CN}. Based on these values roughly half of CN particles become activated at 0.2% supersaturation over ENP and the ratios (CN/CCN) remain nearly constant except for relatively high values near LA due to small-sized recently formed particles. Understanding this horizontal distribution of aerosols can allow for better representation in model and cloud interaction studies.
2. The CCN retrieval methods developed in Ghan and Collins (2004) and Ghan et al. (2006) are used in this study using the ship-based N_{CCN} measurements as a constraint. The uncertainty of the retrieved N_{CCN} profiles is estimated based on the inputs of HSRL measurements and dry factor *f(RH,z)*. These measurements give an estimated uncertainty of ±12.5 cm $^{-3}$ for N_{CCN}. The assumptions used in the retrieval process are discussed and partially proved from the MAGIC measurements. For instance, we use the surface N_{CCN}, wind speed,

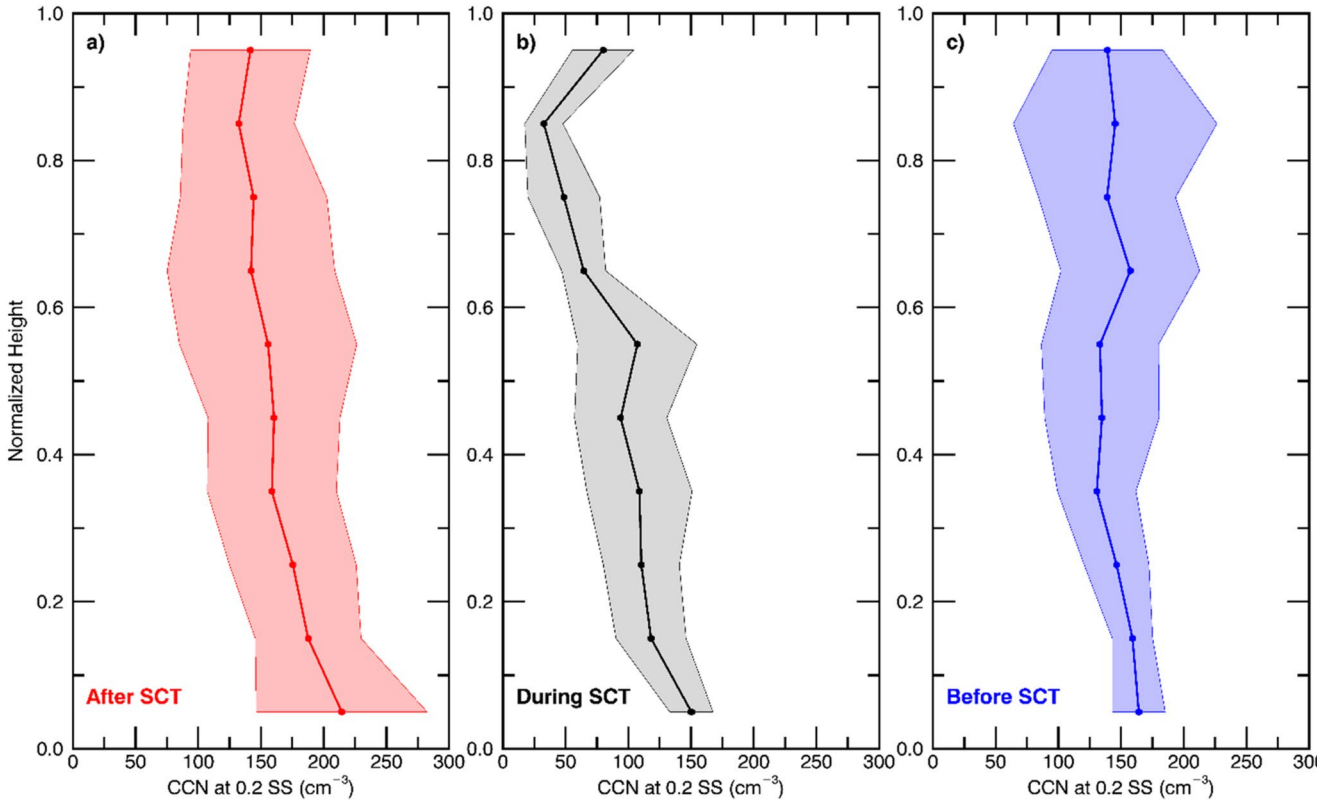

Figure 8. Normalized mean $N_{CCN,0.2}$ from the surface to the cloud base; (a) averaged over 2° longitude 1–3° after (west) the SCT, (b) averaged over 2° longitude during the SCT, and (c) averaged over 2° longitude 1–3° before (east) the SCT. Legs 14B, 15A, and 18B were used in this figure.

backscatter, cloud-droplet number concentration N_c, and the lowest HSRL backscatter (150 m) measurements to validate the assumption, the lowest HSRL backscatter is the same as the surface backscatter during the warm months of MAGIC field campaign.

3. There are a total of 1,295 retrieved N_{CCN} profiles during MAGIC, including 325 cases (25.1%) for clear-sky conditions (no clouds), 556 cases (42.9%) for non-drizzling clouds, and 414 cases (32.0%) for virga. For both cloud and virga cases, N_{CCN} profiles were retrieved from the surface to cloud base. Based on all cloudy samples, we classify these samples into coupled (250 samples) and decoupled (720) conditions. The decoupled $N_{CCN,0.2}$ decrease by ~25 cm^{-3} (~20%) from the surface to cloud base, whereas the coupled $N_{CCN,0.2}$ values decrease by ~20 cm^{-3} (~14%) and show higher concentrations than the decoupled values. The higher *NCCN,0.2* and less decrease from the surface to cloud base under coupled conditions make physical sense and demonstrate that the previous assumptions are mostly valid for coupled conditions, while it should be used with caution for decoupled conditions.
4. In order to better understand the relationship between the retrieved N_{CCN} profiles with the surface N_{CCN} and cloud-droplet number concentration (N_C), we normalized the N_{CCN} profiles from the surface to cloud base from all cloudy N_{CCN} profiles. The correlations between the retrieved N_{CCN} profiles and N_C increase from 0.26 at the surface to 0.38 near cloud base for coupled conditions. Although the correlations are lower than what we expected, the percentage increase (46.2%) is encouraging. This result indicates that the N_{CCN} values near cloud base are more representative than using surface N_{CCN} and should be used to study ACIs in the future. However, a further assessment of the feasibility of this method will be performed at other oceanic locations, where the collocation of ground based retrieved N_{CCN} and aircraft measured N_{CCN} profiles are available.
5. While it is a well-known fact that dynamic forcings play an important role in CB, the environmental conditions associated with CB and its impacts on surface aerosols have not been investigated extensively. In this study, we found that the decreased N_{CN}/N_{CNN} trend east of CB is likely caused by Sc precipitation scavenging, while the increased N_{CN}/N_{CNN} trend west of CB strongly associates with the increased surface wind speed and fewer

drizzle events. However, it is a challenge to tell that the minima CN and CCN concentrations during CB are causes or effects of the SCT. A further study is needed using high-resolution models to simulate these events.

Data Availability Statement

MAGIC data sets can be downloaded from ARM archive available at https://adc.arm.gov/discovery/#/results/site_code::mag. Furthermore, retrieved data set shown and analyzed in this paper here can be accessed by contacting the corresponding author.

Acknowledgments
Atmospheric Radiation Measurement (ARM) Program sponsored by the U.S. Department of Energy (DOE) Office of Energy Research, Office of Health and Environmental Research, and Environmental Sciences Division. This research was supported as part of the "Enabling Aerosol-cloud interactions at Global convection-permitting Scales (EAGLES)" project (74358), funded by the U.S. Department of Energy, Office of Science, Office of Biological and Environmental Research, Earth System Modeling program with the subcontract to the University of Arizona.

References

Albrecht, B. A. (1989). Aerosols, cloud microphysics, and fractional cloudiness. *Science*, *245*(4923), 1227–1230. https://doi.org/10.1126/science.245.4923.1227

Brendecke, J., Dong, X., Xi, B., & Wu, P. (2021). Maritime cloud and drizzle microphysical properties retrieved from ship-based observations during MAGIC. *Earth and Space Science*, *8*, e2020EA001588. https://doi.org/10.1029/2020EA001588

Bretherton, C. S., & Wyant, M. C. (1997). Moisture transport, lower-tropospheric stability, and decoupling of cloud-topped boundary layers. *Journal of the Atmospheric Sciences*, *54*, 148–167. https://doi.org/10.1175/1520-0469(1997)054<0148:MTLTSA>2.0.CO;2

Bretherton, C. S., Wood, R., George, R. C., Leon, D., Allen, G., & Zheng, X. (2010). Southeast Pacific stratocumulus clouds, precipitation and boundary layer structure sampled along 20° S during VOCALS-REx. *Atmospheric Chemistry and Physics*, *10*(21), 10639–10654. https://doi.org/10.5194/acp-10-10639-2010

Dong, X., Xi, B., & Wu, P. (2014). Investigation of the diurnal variation of marine boundary layer cloud microphysical properties at the Azores. *Journal of Climate*, *27*(23), 8827–8835. https://doi.org/10.1175/JCLI-D-14-00434.1

Dong, X. Q., Schwantes, A. C., Xi, B. K., & Wu, P. (2015). Investigation of the marine boundary layer cloud and CCN properties under coupled and decoupled conditions over the Azores. *Journal of Geophysical Research: Atmospheres*, *120*, 6179–6191. https://doi.org/10.1002/2014JD022939

Eloranta, E. W. (2005). High spectral resolution lidar. In K. Weitkamp (Ed.), *Lidar: Range-resolved optical remote sensing of the atmosphere*, *Springer Ser. in Opt. Sci.* (pp. 143–163). Springer.

Feingold, G., & Grund, C. J. (1994). Feasibility of using multiwavelength lidar measurements to measure cloud condensation nuclei. *Journal of Atmospheric and Oceanic Technology*, *11*, 15432–15586. https://doi.org/10.1175/1520-0426(1994)011%3C1543FOUMLM%3E2.0

Gasso, S., Hegg, D. A., Covert, D. S., Collins, D., Noone, K. J., Ostrom, E., et al. (2000). Influence of humidity on the aerosol scattering coefficient and its effect on the upwelling radiance during ACE-2. *Tellus Series B*, *52*, 546–567. https://doi.org/10.1034/j.1600-0889.2000.00055.x

Ghan, S. J., & Collins, D. R. (2004). Use of in situ data to test a Raman lidar-based cloud condensation nuclei remote sensing method. *Journal of Atmospheric and Ocean Technology*, *21*, 387–394. https://doi.org/10.1175/1520-0426(2004)021<0387:uoisdt>2.0.co;2

Ghan, S. J., Rissman, T. A., Elleman, R., Ferrare, R. A., Turner, D., Flynn, C., et al. (2006). Use of in situ cloud condensation nuclei, extinction, and aerosol size distribution measurements to test a method for retrieving cloud condensation nuclei profiles from surface measurements. *Journal of Geophysical Research*, *111*, https://doi.org/10.1029/2004JD005752

Jones, C., Bretherton, C., & Leon, D. (2011). Coupled versus decoupled boundary layers in VOCALS-REx. *Atmospheric Chemistry and Physics*, *11*, 7143–7153. https://doi.org/10.5194/acp-11-7143-2011

Junge, C. (1952). Gesetzmäßigkeiten in der größenverteilung atmosphärischer aerosole über dem kontinent. *Berichte des Deutschen Wetterdienstes*, *35*, 261–277.

Köhler, H. (1936). The nucleus in and the growth of hygroscopic droplets. *Transactions of the Faraday Society*, *32*, 1152–1161. https://doi.org/10.1039/tf9363201152

Latham, J., Bower, K., Choularton, T., Coe, H., Connolly, P., Cooper, G., et al. (2012). Marine cloud brightening. *Philosophical Transactions of the Royal Society A: Mathematical, Physical & Engineering Sciences*, *370*(1974), 4217–4262. https://doi.org/10.1098/rsta.2012.0086

Logan, T., Xi, B., & Dong, X. (2014). Aerosol properties and their influences on marine boundary layer cloud condensation nuclei at the ARM mobile facility over the Azores. *Journal of Geophysical Research: Atmospheres*, *119*(8), 4859–4872. https://doi.org/10.1002/2013JD021288

Lv, M., Wang, Z., Li, Z., Luo, T., Ferrare, R., Liu, D., et al. (2018). Retrieval of cloud condensation nuclei number concentration profiles from lidar extinction and backscatter data. *Journal of Geophysical Research: Atmospheres*, *123*, 6082–6098. https://doi.org/10.1029/2017JD028102

Mather, J. H., & Voyles, J. W. (2013). The ARM climate research facility: A review of structure and capabilities. *Bulletin of the American Meteorological Society*, *94*, 377–392. https://doi.org/10.1175/BAMS-D-11-00218.1

Miller, M. A., Nitschke, K., Ackerman, T. P., Ferrell, W. R., Hickmon, N., & Ivey, M. (2016). The ARM mobile facilities. *Meteorological Monographs*, *57*, 91–915. https://doi.org/10.1175/amsmonographs-d-15-0051.1

Monahan, E. C., Fairall, C. W., Davidson, K. L., & Boyle, P. J. (1983). Observed inter-relations between 10 m winds, ocean whitecaps and marine aerosols. *Quarterly Journal of the Royal Meteorological Society*, *109*, 379–392. https://doi.org/10.1002/qj.49710946010

Painemal, D., Chiu, J.-Y. C., Minnis, P., Yost, C., Zhou, X., Cadeddu, M., et al. (2017). Aerosol and cloud microphysics covariability in the northeast Pacific boundary layer estimated with ship-based and satellite remote sensing observations. *Journal of Geophysical Research: Atmospheres*, *122*, 2403–2418. https://doi.org/10.1002/2016JD025771

Painemal, D., Minnis, P., & Nordeen, M. (2015). Aerosol variability, synoptic-scale processes, and their link to the cloud microphysics over the northeast Pacific during MAGIC. *Journal of Geophysical Research: Atmospheres*, *120*, 5122–5139. https://doi.org/10.1002/2015JD023175

Schulze, B. C., Charan, S. M., Kenseth, C. M., Kong, W., Bates, K. H., Williams, W., et al. (2020). Characterization of aerosol hygroscopicity over the Northeast Pacific Ocean: Impacts on prediction of CCN and stratocumulus cloud droplet number concentrations. *Earth and Space Science*, *7*. https://doi.org/10.1029/2020EA001098

Su, W., Schuster, G. L., Loeb, N. G., Rogers, R. R., Ferrare, R. A., Hostetler, C. A., et al. (2008). Aerosol and cloud interaction observed from high spectral resolution lidar data. *Journal of Geophysical Research*, *113*, D24202. https://doi.org/10.1029/2008JD010588

Twomey, S. (1977). The influence of pollution on the shortwave albedo of clouds. *Journal of Atmospheric Science*, *34*(7), 1149–1152. https://doi.org/10.1175/1520-0469(1977)034<1149:TIOPOT>2.0.CO;2

Wang, Y., Zheng, X., Dong, X., Xi, B., Wu, P., Logan, T., & Yung, Y. L. (2020). Impacts of long-range transport of aerosols on marine-boundary-layer clouds in the eastern North Atlantic. *Atmospheric Chemistry and Physics*, *20*, 14741–14755. https://doi.org/10.5194/acp-20-14741-2020

Wu, P., Dong, X., Xi, B., Tian, J., & Ward, D. M. (2020). Profiles of MBL cloud and drizzle microphysical properties retrieved from ground-based observations and validated by aircraft in situ measurements over the Azores. *Journal of Geophysical Research: Atmospheres*, *125*, e2019JD032205. https://doi.org/10.1029/2019JD032205

Wyant, M. C., Bretherton, C. S., Rand, H. A., & Stevens, D. E. (1997). Numerical simulations and a conceptual model of the stratocumulus to trade cumulus transition. *Journal of the Atmospheric Sciences*, *54*(1), 168–192. https://doi.org/10.1175/1520-0469(1997)054<0168:nsaacm>2.0.co;2

Yamaguchi, T., Feingold, G., & Kazil, J. (2017). Stratocumulus to cumulus transition by drizzle. *Journal of Advances in Modeling Earth Systems*, *9*(6), 2333–2349. https://doi.org/10.1002/2017MS001104

Zheng, X., Xi, B., Dong, X., Logan, T., Wang, Y., & Wu, P. (2020). Investigation of aerosol-cloud interactions under different absorptive aerosol regimes using Atmospheric Radiation Measurement (ARM) southern Great Plains (SGP) ground-based measurements. *Atmospheric Chemistry and Physics*, *20*, 3483–3501. https://doi.org/10.5194/acp-20-3483-2020

Zheng, X., Xi, B., Dong, X., Wu, P., Logan, T., & Wang, Y. (2022). Environmental effects on aerosol–cloud interaction in non-precipitating marine boundary layer (MBL) clouds over the eastern North Atlantic. *Atmospheric Chemistry and Physics*, *22*, 335–354. https://doi.org/10.5194/acp-22-335-2022

Zhou, X., Kollias, P., & Lewis, E. (2015). Clouds, precipitation, and marine boundary layer structure during MAGIC. *Journal of Climate*, *28*(6), 2440–2442. https://doi.org/10.1175/jcli-d-14-00320.1